Check for updates

Twin-roll casting of wire of magnesium alloys

Christoph Kaden*, Kristina Kittner, Madlen Ullmann and Ulrich Prahl

Institute of Metal Forming, Technische Universität Bergakademie Freiberg, Freiberg, Germany

Twin-roll casting (TRC) enables the production of near-net-shape semi-finished products in a single forming step, offering significant energy and cost savings compared to conventional rolling. While TRC has been successfully applied to flat magnesium alloy products, its application to long products, such as wires, remains a novel research focus. In this study, the microstructure, texture, and mechanical properties of TRC wires were investigated for the common wrought alloys AZ31 and AZ80, as well as the calcium-containing alloy ZAX210. Microstructural analysis was performed using scanning electron microscopy (SEM) and electron backscatter diffraction (EBSD). Mechanical properties were evaluated through tensile testing at room temperature. The TRC wires exhibited a central segregation zone with a characteristic necklace-like grain structure composed of small and large grains. The addition of Ca in ZAX210 significantly reduced segregation. SEM analysis revealed fine and large network-like intermetallic phases, including $Mg_{17}Al_{12}$, AlMn, and $Ca_2Mg_6Zn_3$. Texture analysis indicated a pole split or a shifted basal pole with low intensities. Tensile testing showed that the increased Al content in AZ80 led to lower mechanical properties compared to AZ31. Both alloys displayed low elongation at fracture due to pronounced central segregation and brittle intermetallic phases. In contrast, ZAX210 exhibited a finer and more homogeneous microstructure, resulting in the highest tensile strength and elongation at fracture. These findings suggest that the TRC process introduces characteristic microstructural features that influence mechanical properties. The observed improvements in ZAX210 highlight the potential of calcium additions to refine the microstructure and mitigate segregation effects.

KEYWORDS

twin-roll casting, AZ31, AZ80, ZAX210, microstructure

1 Introduction

Mg alloys are increasingly attracting attention in a variety of applications. This is due to their low density and high specific strength, making them particularly suitable for saving weight without sacrificing strength. Typical application areas include the automotive industry, aviation, the electrical and sports industries, as well as medicine (Tan and Ramakrishna, 2021; Prasad et al., 2022; Liu et al., 2023). Because of its nearly identical density and elastic modulus compared to human bone tissue, Mg alloys prove to be a promising option for use in implants (Uppal et al., 2022). Mg alloys are also used as a stent, with their good biocompatibility and ability to biologically degrade through corrosion enhancing interest in this material (Ghafari et al., 2023).

In the field of biomedicine, thinner Mg wire are specifically employed (Griebel et al., 2024). The current main methods for producing such wires primarily include caliber rolling

FIGURE 1
Twin-roll casting of wire: process schematic **(A)** twin-roll cast wire profile **(B)** and cross section of the twin-roll cast wire **(C)**.
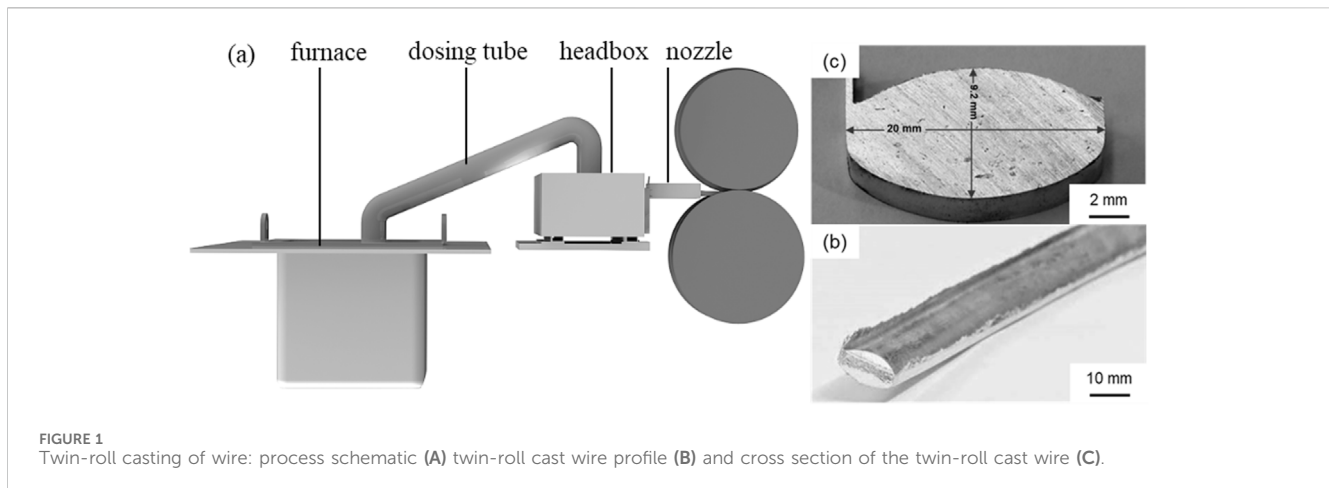
(Kong et al., 2020), drawing (Dodyim et al., 2020) and extrusion (TESAŘ et al., 2020). Twin-roll casting represents another method that enables cost-efficient and energy-saving production (Kawalla et al., 2018). By combining casting and rolling in one step, process times and emissions can be reduced. The basis for twin-roll casting of Mg wire builds upon experiences from twin-roll casting of Mg sheets, a practice that has been in place since the 1980s (Javaid and Czerwinski, 2021). In the field of sheet metal, previous studies have shown that twin-roll casting results in a refinement of the microstructure and a weakening of the texture, which can lead to improved mechanical properties (Neh et al., 2015). The process has already been applied to many different Mg alloys, such as AZ31 (Zimina et al., 2018), WE43 (Neh et al., 2014), ZK60 (Bhattacharjee et al., 2014) and ZEK100 (Máthis et al., 2018). In contrast, twin-roll casting of Mg wire, or wire in general, has been studied to a very limited extent. However, Moses (Moses et al., 2023) and Arndt (Arndt et al., 2022) have also observed a similar grain refinement and texture weakening during the twin-roll casting of an AZ31 alloy wire.

This paper focuses on the twin-roll casting process of wire for the AZ31, AZ80, and ZAX210 alloys. The microstructure, texture, and mechanical properties are investigated and presented. The selection of the alloys was based on their distinct chemical compositions and resulting microstructural and mechanical properties. AZ31 is a widely used wrought Mg alloy known for its good formability and moderate strength (Pekguleryuz, 2012). AZ80, with a higher Al content, exhibits increased precipitation of $Mg_{17}Al_{12}$, which enhances strength but reduces ductility. In contrast, the calcium-containing ZAX210 alloy was included to investigate the role of Ca in modifying the microstructure and texture during twin-roll casting, as it is reported to weaken the texture and improve elongation at fracture (Ding et al., 2015).

2 Materials and methods

The twin-roll cast wires considered for examination were produced at the twin-roll casting plant of the Institute of Metal Forming at the TU Bergakademie Freiberg (Moses et al., 2019). In this process, the Mg alloy is first melted in a furnace under a protective gas and conveyed into a headbox via a dosing tube.

TABLE 1 process parameters for the twin-roll casting.

Parameter	AZ31	AZ80	ZAX210
Furnace temperature [°C]	710	680	690
Dosing tube temperature [°C]	750	750	750
Headbox temperature [°C]	720	690	720
Nozzle temperature [°C]	690	670	700
Setback [mm]	65	65	65
Rolling speed [min^{-1}]	3.5	4.5	4

Subsequently, the melt flows through a hybrid casting nozzle, consisting of steel and ceramic, into the rolling gap between two counter-rotating, water-cooled rolls (Figure 1A). There, it solidifies from the outside in and undergoes initial deformation. To prevent the melt from adhering to the rolls, a release agent consisting of a water-graphite solution was used. The final wire has an oval cross-section of 9.2 mm in height and 20.0 mm in width due to the groove formed by the rolls in the roll gap (Figures 1B, C). For each alloy, approximately 30 m of wire was produced.

Temperature control during the twin-roll casting process is crucial to ensure uniform solidification and stable process conditions. The process temperatures depend, among other factors, on the liquidus and solidus temperatures and the resulting solidification interval of the respective alloy. Generally, the melt is heated in the furnace to a temperature approximately 70 K above the liquidus temperature of the respective alloy. However, the ZAX210 alloy, due to its strong sticking tendency caused by the addition of calcium (Kondori and Mahmudi, 2010), requires special considerations, and a lower furnace temperature was chosen. This decision was based on experience, indicating that less superheating is necessary in this case to ensure process stability and minimize sticking tendencies. In all cases, the temperature of the dosing tube was maintained at a constant 750°C to prevent blockages and deposits. This temperature can be sustained by the system components without causing permanent damage and ensures that the melt remains fluid as it is transported to the next stage of the process. In the headbox, the melt's temperature was maintained to compensate for any heat losses during transfer. For AZ31 and

TABLE 2 chemical composition of the AZ31, AZ80 and ZAX210 ingots determined by optical emission spectroscopy (wt%).

	Al	Zn	Mn	Ca	Si	Fe	Ni	Mg
AZ31	2.880	0.985	0.337	<0.001	0.008	0.002	<0.001	Bal
AZ80	8.370	0.355	0.200	<0.001	0.018	0.006	<0.001	Bal
ZAX210	0.741	2.000	0.037	>0.180	0.008	0.006	0.003	Bal

ZAX210, the temperature was set at 720°C to maintain sufficiently high melt temperatures, while for AZ80, a lower temperature of 690°C was chosen, consistent with its lower liquidus temperature. The nozzle temperature was selected to keep the melt fluid enough to allow for even distribution into the rolling gap without premature solidification. The setback (distance between the nozzle and the rolling gap) and the profile height are two constant influencing factors. The twin-roll casting speed (wire speed) is controlled by the roll speed. The highest speeds were required for the AZ80 alloy, as lower speeds led to cracking. A selection of the most important parameters used is shown in Table 1.

The twin-roll cast alloys include the two standard wrought alloys AZ31 and AZ80 (Friedrich and Mordike, 2006) as well as the Ca-containing ZAX210 alloy (Neh et al., 2016). In addition to the main alloying elements Al, Zn and Mn, Si, Fe and Ni are also included. Al and Zn improve strength (Loukil, 2022), while Mn increases

corrosion resistance and Si increases the creep properties (Mohammadi Mazraeshahi et al., 2015; Loukil, 2022). Fe, on the other hand, have a detrimental effect on corrosion behavior and must be kept below a critical threshold, often below 0.005 wt% (Yang et al., 2018). The Ca content in the ZAX210 alloy results in grain refinement, which increases creep resistance and improves formability due to the weakening of the rolling texture (Ullmann et al., 2019). The chemical compositions of the twin-roll cast alloys are listed in Table 2.

To investigate the microstructure and texture analysis, the wire was separated, embedded, ground with silicon carbide paper and polished with an oxide polishing suspension. It was then etched with a solution of 70 mL ethanol, 10 mL glacial acetic acid, 4.2 g picric acid and 10 mL distilled water. The Keyence VHX-6000 optical microscope and the ZEISS GeminiSEM 450 scanning electron microscope were used to evaluate the microstructure of the longitudinal section. The chemical composition of individual microstructural constituents was analyzed using energy dispersive X-ray spectroscopy (EDX). Acceleration voltage of 20 kV and a working distance of 8.5 mm were applied. The texture measurements were carried out with the Electron Backscatter Diffraction (EBSD) Detector. The voltage used for acquisition of EBSD data was 15–20 kV, and the step size was 0.65 μm. The analysis of the EBSD data and the calculation of the pole figures were carried out using the MTEX MATLAB toolbox (version 5.9.0,
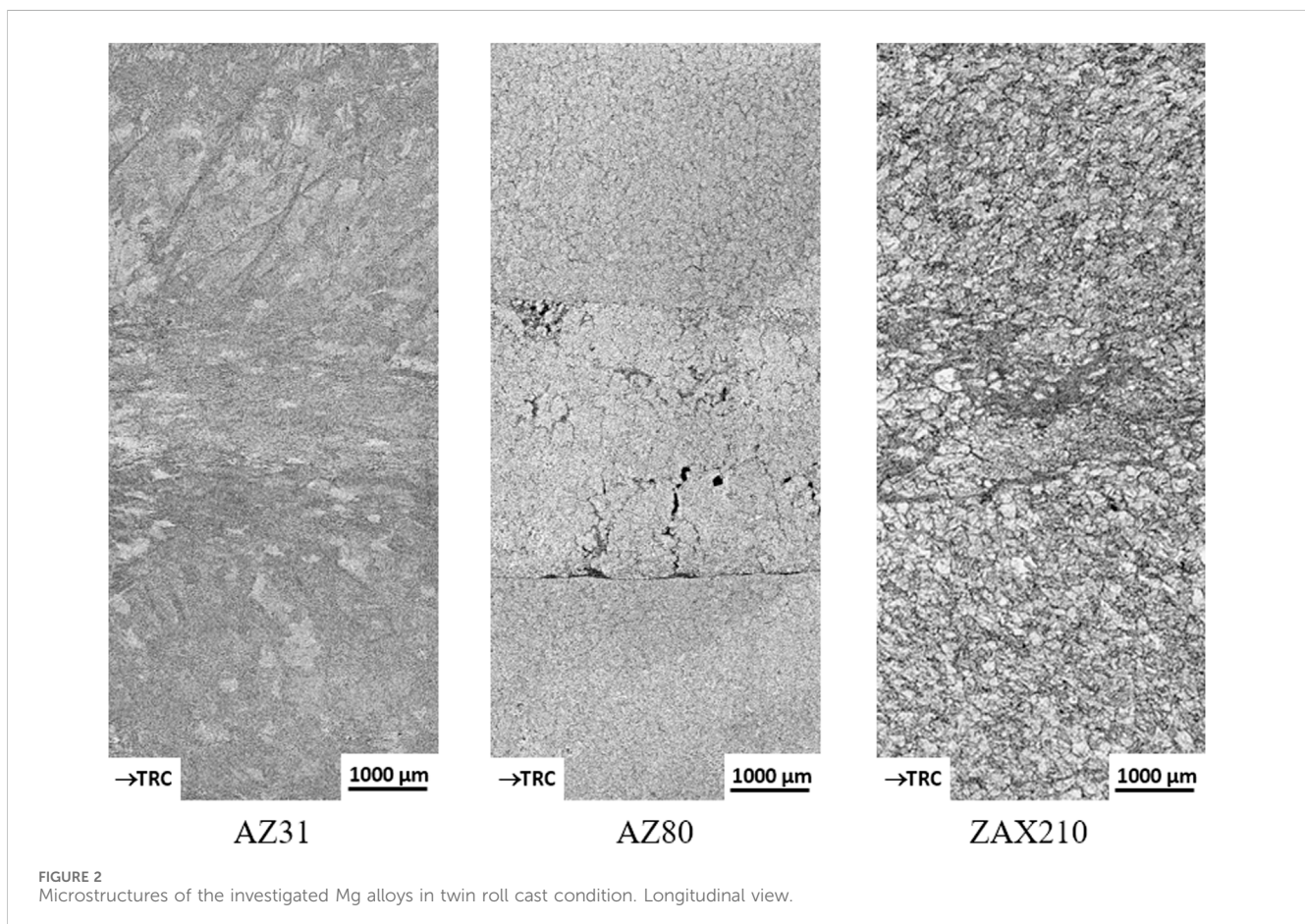
FIGURE 2
Microstructures of the investigated Mg alloys in twin roll cast condition. Longitudinal view.
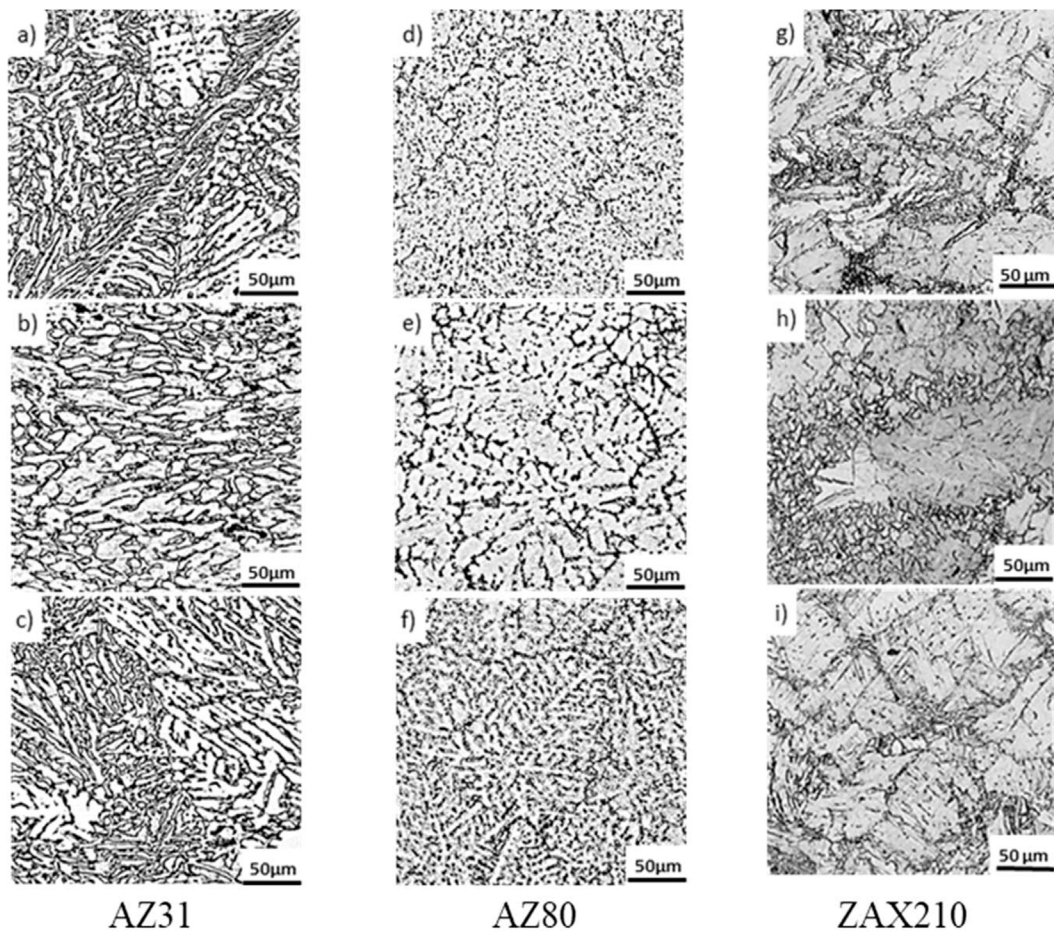
FIGURE 3
Detailed images of the microstructures of the investigated Mg alloys from the top **(A, D, G)**, the middle **(B, E, H)** and the bottom **(C, F, I)** of the longitudinal view.

MTEX, Ralf Hielscher, Freiberg, Germany) (Bachmann et al., 2010). For tensile tests, tensile specimens correspond to DIN 50125 shape B with a gauge diameter of 5 mm and a gauge length of 25 mm were machined and used. For each alloy, six tensile tests were performed at room temperature and a traverse speed of 0.625 mm/min.

3 Results and discussion

The twin-roll cast wires were characterized regarding their microstructure, chemical composition, and mechanical properties. Figure 2 shows the overview images of the etched samples of the respective alloys in longitudinal section. Upon contact of the melt with the rolls, a fine edge layer with small grains forms due to the high cooling rate. Due to the heat transfer into the center of the wire, stem-like dendrites form, which are redirected in the direction of the heat flow due to roll rotation (Figure 3). Because of the high cooling rate, there is no time for diffusion processes, leading to the enrichment of the residual melt with alloying elements. The meeting of solidification fronts forms the segregation zone. This zone consists of a coarse, inhomogeneous cast structure with an increased proportion of intermetallic phases, which are unevenly

distributed. This typical structure was already observed by Arndt et al., (2022) in the investigation of a twin-roll cast wire of the AZ31 alloy. A similar structure also forms during the twin-roll casting of Mg sheets (Neh et al., 2015). In the case of the AZ80 alloy, it also leads to a formation of an inverse segregation in the center of the wire. Inverse segregation occurs when a highly alloyed liquid phase becomes trapped in the central region of the wire and is subsequently pushed outward toward the wire surface by the roll separating force. This phenomenon is intensified by hydrodynamic effects generated by the rotating rollers, resulting in a non-uniform composition and microstructure (Ullmann et al., 2024). In the case of alloys with a wider solidification range, such as AZ80, the inverse segregations are more pronounced (Park et al., 2007). In the ZAX210 alloy, the segregation region is less pronounced compared to the AZ alloys, only occasional local segregation formation can be observed. Additionally, the structure is notably more homogeneous. The detailed images in Figure 3 also show that the fine dendritic structure is interspersed with small grains and twins.

The region of the segregation zone and the edge area were further examined using scanning electron microscopy. The Mg matrix is depicted in dark, while precipitates appear brighter.
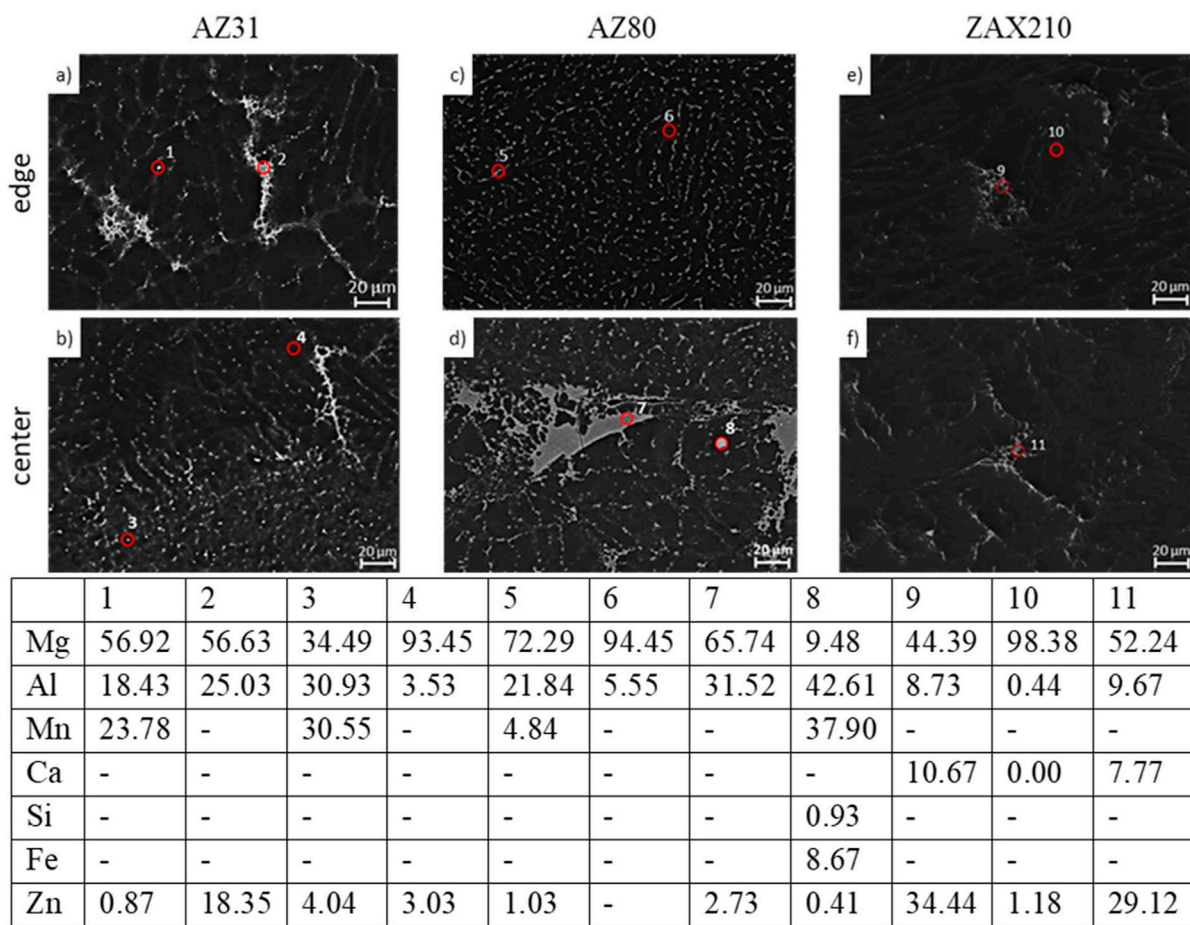
FIGURE 4
EDS measurement of the edge **(A, C, E)** and the center **(B, D, F)** with the chemical composition of selected points of the twin-roll cast alloys (wt%).

	1	2	3	4	5	6	7	8	9	10	11
Mg	56.92	56.63	34.49	93.45	72.29	94.45	65.74	9.48	44.39	98.38	52.24
Al	18.43	25.03	30.93	3.53	21.84	5.55	31.52	42.61	8.73	0.44	9.67
Mn	23.78	-	30.55	-	4.84	-	-	37.90	-	-	-
Ca	-	-	-	-	-	-	-	-	10.67	0.00	7.77
Si	-	-	-	-	-	-	-	0.93	-	-	-
Fe	-	-	-	-	-	-	-	8.67	-	-	-
Zn	0.87	18.35	4.04	3.03	1.03	-	2.73	0.41	34.44	1.18	29.12

Starting with AZ31, the local chemical composition in Figure 4 (point 4), shows that Al and Zn are dissolved in the Mg solid solution, while Mn cannot be detected in the matrix. The mass fraction of Al is 3.53% and that of zinc is 3.03%. Furthermore, large network-like phases are visible. A point analysis for Point 2 reveals an Al content of 25.03% and a Zn content of 18.35%. Based on the chemical composition and comparison with the literature (Sheikhani et al., 2022), this is likely to be the $Mg_{17}(Al, Zn)_{12}$ phase, commonly found in AZ alloys. It is also evident that Mn appears exclusively in finely dispersed, rounded precipitates (point 1 and 3). Moreover, large amounts of Al are contained in the Mn-rich phases, suggesting the presence of the AlMn phase. The distribution and size of the precipitates are similar in the center and edge regions. In the case of the AZ80 alloy, the images of the center region (Figure 4, d) again show a mixture of fine and coarse, network-like precipitates. The Mg matrix consists of Mg (94.45%) and Al (5.55%), with no presence of Zn and Mn. Measurement of the local chemical composition in the area of the large bright phase (point 7) shows an increase in Al content to 31.52% and Zn content to 2.73%. Additionally, at Point 8, alongside 37.90% Mn, 8.67% Fe and 0.93% Si were measured. Fe particles can occur in the melt due to the manufacturing process, although Fe significantly worsens the corrosion resistance. The addition of Mn in Mg alloys has the advantage of binding Fe particles through the formation of Fe-Mn-containing compounds, thereby mitigating their negative effect on the alloy's corrosion resistance (Simanjuntak et al., 2015). Furthermore, in contrast to the wire center, the precipitates in the edge region (c) are very fine and evenly distributed. Small round phases, where Mn is dissolved, are also observed here (point 5). In the case of the ZAX210 alloy, the Mg matrix contains only a small amount of Al and Zn, with no dissolved Ca (Figure 4, point 10). The precipitates, especially in the wire center, again appear in network-like structures, but are finer compared to the AZ alloys. The chemical composition of the phase at Point 11 shows a high Zn content of 29.12% and similar contents of Al (9.67%) and Ca (7.77%). According to the literature, this is likely to be the $Mg_6Ca_2Zn_3$ phase (Katsarou et al., 2016).

Figure 5 shows regions within the segregation zone, their {0001} pole figures and the misorientation angle distributions. The inverse pole figure (IPF) map reveals inhomogeneous grain structures consisting of small and large grains, with the small recrystallized grains forming along the grain boundaries. This so-called necklace structure indicates that discontinuous dynamic recrystallization is the dominant recrystallization mechanism (Chen et al., 2022). Twins are also recognizable, especially in the ZAX210 alloy. The misorientation angle distribution allows for an assessment of the

FIGURE 5
Results of EBSD analysis of the twin roll cast wires within the segregation zone: inverse pole figure maps **(A, D, G)**, misorientation angle distribution **(B, E, H)**, {0001} pole figures **(C, F, I)**.
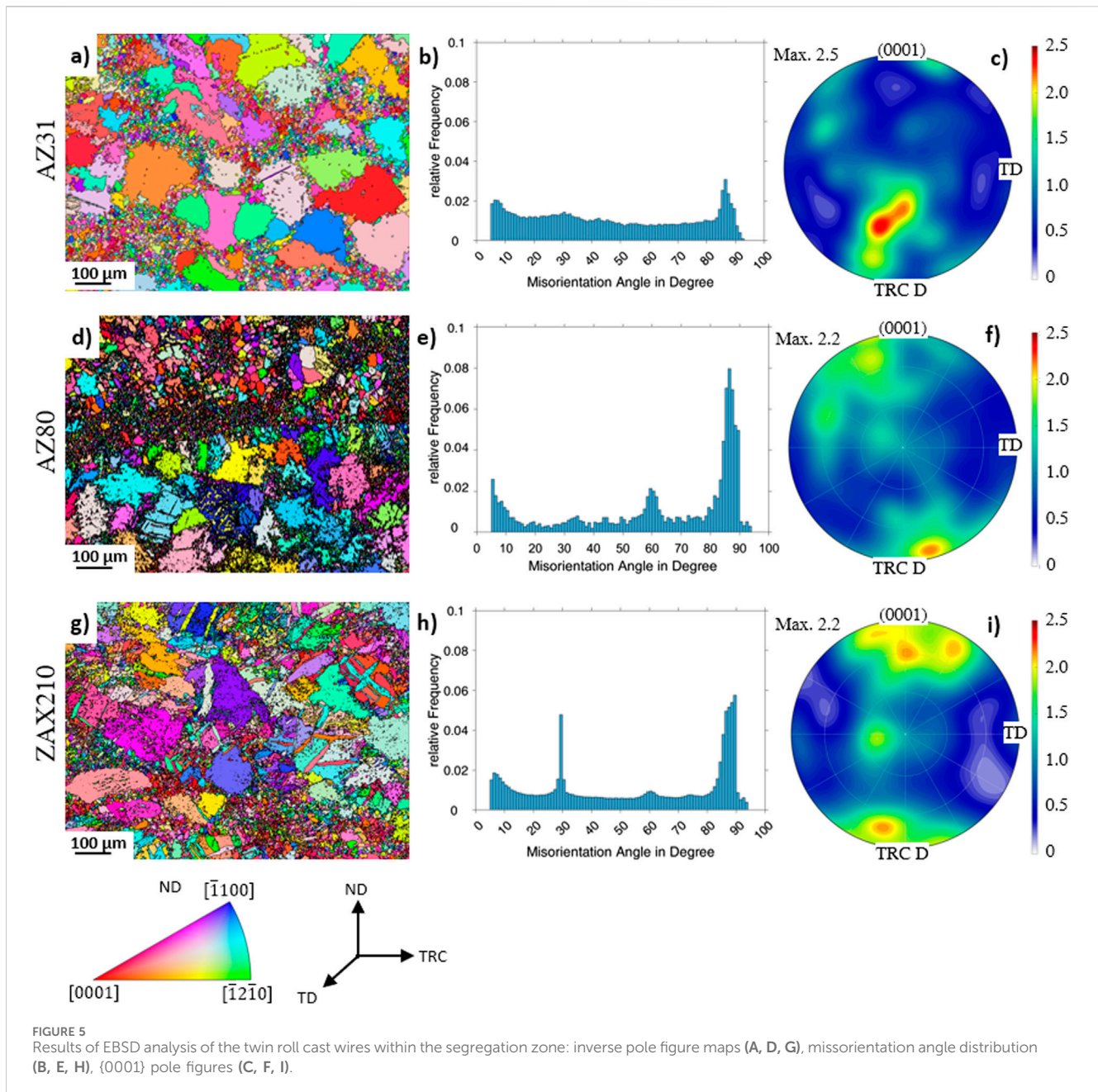
dominant twinning systems. All three alloys exhibit the highest peak between 85° and 90°, indicative of {10 $\bar{1}$ 2} tensile twins. These twins often occur during the deformation of Mg alloys and can be activated even at low deformation levels due to their low critical resolved shear stress (CRSS) (C. Zhang et al., 2023). Another notable peak occurs in the AZ80 alloy between 56° and 65°, suggesting the presence of {10 $\bar{1}$ 1} or {10$\bar{1}$ 3} compression twins. This peak is very weak in the ZAX210 alloy and not observed in AZ31. Furthermore, a distinct peak at just below 30° is observed in the ZAX210 alloy, which cannot be attributed to any twinning system. Instead, this type of grain boundary is most likely generated by the rotation of grains driven by dislocation slip (Li et al., 2015). The {0001} pole figure of the AZ31 alloy shows a shift of the basal pole in the rolling direction.

The maximum intensity is low at 2.5, indicating a weakened texture. When considering the {0001} pole figures of the AZ80 and ZAX210 alloys, a non-basal texture with a pole split is observed, with the maximum intensities inclined in the direction of twin-roll casting. This intensity split is also typical for rolled Mg alloys (Nie et al., 2020). According to Zecevic et al. (2018), activation of pyramidal slip leads to texture splitting in the rolling direction. In addition, Onuki et al. (2015) consider the formation of tensile twins to be necassary. The splitting is more pronounced in ZAX210, although the lower maximum intensities also suggest a weakened texture here. The generally lower texture intensities observed in AZ80 and ZAX210 can also be attributed to the higher fraction of recrystallized grains. Discontinuous dynamic recrystallization

FIGURE 6
Mechanical properties of the investigated Mg alloys in twin-roll cast condition.
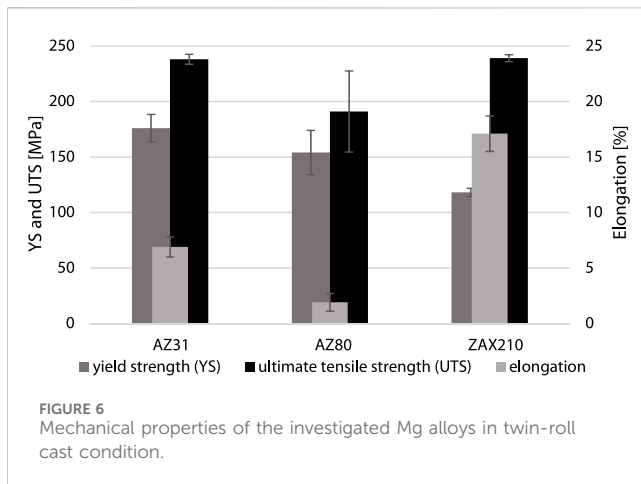
(DDRX) is known for randomizing the grain orientation and weakening the basal texture (Zhang et al., 2023). Furthermore, as is already known for extruded sheets, the addition of Ca contributes to the weakening and modification of the texture (Ding et al., 2015). The textures observed in the investigated alloys differ significantly from those commonly reported for twin-roll cast Mg sheets, as well as conventionally processed Mg wires. Twin-roll cast sheets typically exhibit a strong basal texture, with the c-axis oriented perpendicular to the rolling plane as a result of plane strain deformation (Kittner et al., 2019). Drawn Mg wires develop a characteristic fiber texture, where the basal poles align parallel to the drawing direction due to the high axisymmetric deformation involved in the process (Chatterton et al., 2014). In contrast, twin-roll cast Mg wires exhibit either a basal pole split (AZ31) or a splitting of the maximum intensity into multiple peaks (AZ80, ZAX210), both characterized by overall low texture intensities. These differences can be attributed to the lower deformation levels in the wire center and the influence of solidification structures such as centerline segregation.

The mechanical properties, including yield strength (YS), ultimate tensile strength (UTS), and elongation at fracture, determined from the tensile tests at room temperature, are presented in Figure 6. Compared to the other alloys, AZ31 exhibits the highest values for YS (176 MPa), but the elongation at fracture is relatively low at 6.9%. AZ80 shows overall lower values compared to AZ31, with an elongation at fracture of only 1.9%. The ZAX210 alloy demonstrates the highest tensile strength at 239 MPa and the highest elongation at fracture at 17.1%, but the lowest yield strength at 118 MPa. One possible reason for the high tensile strength and, especially, the high elongation at fracture observed in ZAX210 could be the addition of calcium. This would be align with Bhattacharjee et al. (2014), who noted that Ca addition in Mg alloys improved both mechanical properties and processability through grain refinement. Similarly, Wang et al. (2020) highlighted the beneficial effects of Ca in enhancing strength and ductility. Furthermore, the relatively low number of precipitates observed, due to the significantly lower aluminum content, indicates that the microstructure retains its ductility. The lower elongation at fracture observed in the AZ alloys may be attributed to the increased presence of the $Mg_{17}Al_{12}$ phase in the

segregation zone. Due to its brittle behavior, this phase adversely affects the ductility of Mg alloys. Additionally, the alloying content in AZ80, and consequently the proportion of segregation, is significantly higher than that of AZ31, which restricts the plastic deformation. Moreover, voids and cracks occur along and within the segregation zone, further contributing to a reduction in elongation at fracture (Krbetschek et al., 2016). Regarding the ZAX210 alloy, the homogeneous microstructure with already recrystallized regions positively influences the elongation at fracture. Simultaneously, the fine microstructure enhances the tensile strength. The unexpectedly low UTS of AZ80 contrasts with theoretical expectations, as its higher aluminum content compared to ZAX210 typically enhances tensile strength by promoting solid solution strengthening and the precipitation of $Mg_{17}Al_{12}$ phases. However, the severe segregation and resulting structural weaknesses appear to have counteracted this advantage, reducing the effective load-bearing capacity of the alloy under tensile loading.

4 Conclusion

Within this study, the microstructure, texture, and mechanical properties of twin-roll cast wires of the AZ31, AZ80, and ZAX210 alloys were investigated. The findings of this study can be summarized as follows.

(1) Twin-roll casting results in a microstructure characterized by a central segregation zone, wherein both small and large grains form a necklace-like structure. The addition of Ca significantly reduces the extent of the segregation zone in ZAX210.

(2) SEM analysis reveals the presence of both fine and large network-like intermetallic phases. While the phases in the central and outer regions of AZ31 are similar in size and nature, those in AZ80 and ZAX210 are smaller and more finely distributed in the edge region. Mainly, these phases consist of $Mg_{17}Al_{12}$, AlMn, and $Ca_2Mg_6Zn_3$.

(3) No pronounced texture is observed in any of the three alloys. The pole figures of AZ80 and ZAX210 exhibit pole splits with the inclination of intensity maxima in the twin-roll casting direction, whereas the basal pole of AZ31 is shifted in the twin-roll casting direction. Overall, however, the intensity maxima are very low.

(4) Tensile tests at room temperature indicate that the mechanical properties of the AZ80 alloy deteriorate due to the increased addition of Al compared to AZ31. The elongation at fracture is very low in both alloys due to the prominent central segregation, the inverse segregations and the widespread brittle intermetallic phase $Mg_{17}Al_{12}$. In contrast, the addition of Ca in the ZAX210 alloy and the fewer precipitates, due to the lower aluminum content, results in a finer and more homogeneous microstructure, leading to the highest tensile strength and elongation at fracture.

(5) By optimizing the processing conditions, it may be possible to further enhance and fine-tune the overall properties. Future studies are therefore necessary to systematically investigate

the interactions between process parameters, alloying elements, and material properties.

Data availability statement

The original contributions presented in the study are included in the article/supplementary material, further inquiries can be directed to the corresponding author.

Author contributions

CK: Conceptualization, Formal Analysis, Investigation, Methodology, Visualization, Writing–original draft. KK: Conceptualization, Methodology, Validation, Writing–review and editing. MU: Conceptualization, Validation, Writing–review and editing. UP: Supervision, Writing–review and editing.

Funding

Conflict of interest

The authors declare that the research was conducted in the absence of any commercial or financial relationships that could be construed as a potential conflict of interest.

Generative AI statement

The author(s) declare that no Generative AI was used in the creation of this manuscript.

Publisher's note

All claims expressed in this article are solely those of the authors and do not necessarily represent those of their affiliated organizations, or those of the publisher, the editors and the reviewers. Any product that may be evaluated in this article, or claim that may be made by its manufacturer, is not guaranteed or endorsed by the publisher.

References

Arndt, F., Berndorf, S., Moses, M., Ullmann, M., and Prahl, U. (2022). Microstructure and hot deformation behaviour of twin-roll cast AZ31 magnesium wire. *Crystals* 12, 173. doi:10.3390/cryst12020173

Bachmann, F., Hielscher, R., and Schaeben, H. (2010). Texture analysis with MTEX – free and open source software toolbox. *SSP* 160, 63–68. doi:10.4028/www.scientific.net/SSP.160.63

Bhattacharjee, T., Suh, B.-C., Sasaki, T. T., Ohkubo, T., Kim, N. J., and Hono, K. (2014). High strength and formable Mg–6.2Zn–0.5Zr–0.2Ca alloy sheet processed by twin roll casting. *Mater. Sci. Eng. A* 609, 154–160. doi:10.1016/j.msea.2014.04.058

Chatterton, M., Robson, J., and Henry, D. (2014). "Texture evolution during wire drawing of Mg-RE alloy," in *Magnesium technology 2014*. Editors M. Alderman, M. V. Manuel, N. Hort, and N. R. Neelameggham (Wiley), 251–256.

Chen, X., Li, X., Ning, F., Liao, Q., Le, Q., Zhou, X., et al. (2022). The hot rolling deformation performance of as-cast AZ80 magnesium alloy after ultrasonic processing. *J. Mater. Res. Technol.* 17, 1707–1715. doi:10.1016/j.jmrt.2022.01.116

Ding, H., Shi, X., Wang, Y., Cheng, G., and Kamado, S. (2015). Texture weakening and ductility variation of Mg–2Zn alloy with CA or RE addition. *Mater. Sci. Eng.* 645, 196–204. doi:10.1016/j.msea.2015.08.025

Dodyim, N., Yoshida, K., Murata, T., and Kobayashi, Y. (2020). Drawing of magnesium fine wire and medical application of drawn wire. *Procedia Manuf.* 50, 271–275. doi:10.1016/j.promfg.2020.08.050

Friedrich, H. E., and Mordike, B. L. (2006). *Magnesium technology: metallurgy, design data, applications*. Berlin/Heidelberg: Springer-Verlag.

Ghafari, C., Brassart, N., Delmotte, P., Brunner, P., Dghoughi, S., and Carlier, S. (2023). Bioresorbable magnesium-based stent: real-world clinical experience and feasibility of follow-up by coronary computed tomography: a new window to look at new scaffolds. *Biomedicines* 11, 1150. doi:10.3390/biomedicines11041150

Griebel, A. J., David, C. J., Schaffer, J. E., He, W., and Guillory, R. (2024). "Assessment of magnesium wire coatings for absorbable medical devices," in *Magnesium technology 2024*. Editors A. Leonard, S. Barela, N. R. Neelameggham, V. M. Miller, and D. Tolnai (Cham: Springer Nature Switzerland), 187–191.

Javaid, A., and Czerwinski, F. (2021). Progress in twin roll casting of magnesium alloys: a review. *J. Magnesium Alloys* 9, 362–391. doi:10.1016/j.jma.2020.10.003

Katsarou, L., Suresh, K., Rao, K. P., Hort, N., Blawert, C., Mendis, C. L., et al. (2016). "Microstructure and properties of magnesium alloy Mg-1Zn-1Ca (ZX11)," in

Magnesium technology 2015. Editors M. V. Manuel, A. Singh, M. Alderman, and N. R. Neelameggham (Cham: Springer International Publishing), 419–423.

Kawalla, C., Berkel, W., Kawalla, R., Höck, M., and Ligarski, M. (2018). Material flow cost accounting analysis of twin-roll casting magnesium strips. *Procedia Manuf.* 15, 193–200. doi:10.1016/j.promfg.2018.07.194

Kittner, K., Kaden, C., Ullmann, M., and Prahl, U. (2024). Production of AZ80 magnesium alloy wires: influence of heat treatment on microstructure and properties after twin-roll casting. *Prod. Eng. Res. Devel.* doi:10.1007/s11740-024-01310-1

Kittner, K., Ullmann, M., Henseler, T., Kawalla, R., and Prahl, U. (2019). Microstructure and hot deformation behavior of twin roll cast Mg-2Zn-1Al-0.3Ca alloy. *Mater. (Basel)* 12, 1020. doi:10.3390/ma12071020

Kondori, B., and Mahmudi, R. (2010). Effect of Ca additions on the microstructure, thermal stability and mechanical properties of a cast AM60 magnesium alloy. *Mater. Sci. Eng. A* 527, 2014–2021. doi:10.1016/j.msea.2009.11.043

Kong, T., Kwak, B. J., Kim, J., Lee, J. H., Park, S. H., Kim, J. H., et al. (2020). Tailoring strength-ductility balance of caliber-rolled AZ31 Mg alloy through subsequent annealing. *J. Magnesium Alloys* 8, 163–171. doi:10.1016/j.jma.2019.11.005

Krbetschek, C., Berge, F., Oswald, M., Ullmann, M., and Kawalla, R. (2016). "Microstructure investigations of inverse segregations in twin-roll cast AZ31 strips," in *Magnesium technology 2016*. Editors A. Singh, K. Solanki, M. V. Manuel, and N. R. Neelameggham (Cham: Springer International Publishing), 369–374.

Li, B., Liao, M., Ma, Q., and McClelland, Z. (2015). Structure of grain boundaries with 30°[0 0 0 1] misorientation in dynamically recrystallized magnesium alloys. *Comput. Mater. Sci.* 101, 175–180. doi:10.1016/j.commatsci.2015.01.034

Liu, B., Yang, J., Zhang, X., Yang, Q., Zhang, J., and Li, X. (2023). Development and application of magnesium alloy parts for automotive OEMs: a review. *J. Magnesium Alloys* 11, 15–47. doi:10.1016/j.jma.2022.12.015

Loukil, N. (2022). "Alloying elements of magnesium alloys: a literature review," in *Magnesium alloys structure and properties*.

Máthis, K., Horváth, K., Farkas, G., Choe, H., Shin, K. S., and Vinogradov, A. (2018). Investigation of the microstructure evolution and deformation mechanisms of a Mg-Zn-Zr-re twin-roll-cast magnesium sheet by in-situ experimental techniques. *Mater. (Basel)* 11, 200. doi:10.3390/ma11020200

Mohammadi Mazraeshahi, E., Nami, B., Miresmaeili, S. M., and Tabatabaei, S. M. (2015). Effect of Si on the creep properties of AZ61 cast magnesium alloy. *Mater. and Des.* 76, 64–70. doi:10.1016/j.matdes.2015.03.021

Moses, M., Ullmann, M., and Prahl, U. (2023). Twin-roll casting as a grain refinement method and its influence on the microstructure and deformation behavior of an AZ31 magnesium alloy wire. *Crystals* 13, 1409. doi:10.3390/cryst13101409

Moses, M., Wemme, H., Ullmann, M., Kawalla, R., and Prahl, U. (2019). "Twin-roll casting of magnesium wire: an innovative continuous production route," in *METAL 2019 - 28th international conference on metallurgy and materials* (TANGER Ltd), 438–443. doi:10.37904/metal.2019.812

Neh, K., Ullmann, M., and Kawalla, R. (2014). Twin-roll-casting and hot rolling of magnesium alloy WE43. *Procedia Eng.* 81, 1553–1558. doi:10.1016/j.proeng.2014.10.189

Neh, K., Ullmann, M., and Kawalla, R. (2016). Substitution of rare earth elements in hot rolled magnesium alloys with improved mechanical properties. *MSF* 854, 57–64. doi:10.4028/www.scientific.net/MSF.854.57

Neh, K., Ullmann, M., Oswald, M., Berge, F., and Kawalla, R. (2015). Twin roll casting and strip rolling of several magnesium alloys. *Mater. Today Proc.* 2, S45–S52. doi:10.1016/j.matpr.2015.05.013

Nie, J. F., Shin, K. S., and Zeng, Z. R. (2020). Microstructure, deformation, and property of wrought magnesium alloys. *Metall. Mater. Trans.* 51, 6045–6109. doi:10.1007/s11661-020-05974-z

Onuki, Y., Hara, K., Utsunomiya, H., and Szpunar, J. A. (2015). Textures and microstructures formed in WE43 and AZ31 magnesium alloys during high speed rolling and their formation mechanisms. *IOP Conf. Ser. Mater. Sci. Eng.* 82, 012028. doi:10.1088/1757-899X/82/1/012028

Park, S. S., Bae, G. T., Kang, D. H., Jung, I.-H., Shin, K. S., and Kim, N. J. (2007). Microstructure and tensile properties of twin-roll cast Mg–Zn–Mn–Al alloys. *Scr. Mater.* 57, 793–796. doi:10.1016/j.scriptamat.2007.07.013

Pekguleryuz, M. O. (2012). "Current developments in wrought magnesium alloys," in *Advances in wrought magnesium alloys*. Elsevier, 3–62.

Prasad, S. V. S., Prasad, S. B., Verma, K., Mishra, R. K., Kumar, V., and Singh, S. (2022). The role and significance of Magnesium in modern day research-A review. *J. Magnesium Alloys* 10, 1–61. doi:10.1016/j.jma.2021.05.012

Sheikhani, A., Roumina, R., and Mahmudi, R. (2022). Texture softening in a rare earth elements-containing AZ31 magnesium alloy during hot compression deformation. *J. Mater. Res. Technol.* 18, 4089–4098. doi:10.1016/j.jmrt.2022.04.079

Simanjuntak, S., Cavanaugh, M. K., Gandel, D. S., Easton, M. A., Gibson, M. A., and Birbilis, N. (2015). The influence of iron, manganese, and zirconium on the corrosion of magnesium: an artificial neural network approach. *CORROSION* 71, 199–208. doi:10.5006/1467

Tan, J., and Ramakrishna, S. (2021). Applications of magnesium and its alloys: a review. *Appl. Sci.* 11, 6861. doi:10.3390/app11156861

Tesař, K., Balík, K., Sucharda, Z., and Jäger, A. (2020). Direct extrusion of thin Mg wires for biomedical applications. *Trans. Nonferrous Metals Soc. China* 30, 373–381. doi:10.1016/S1003-6326(20)65219-0

Ullmann, M., Kittner, K., Henseler, T., Stöcker, A., Prahl, U., and Kawalla, R. (2019). Development of new alloy systems and innovative processing technologies for the production of magnesium flat products with excellent property profile. *Procedia Manuf.* 27, 203–208. doi:10.1016/j.promfg.2018.12.065

Ullmann, M., Stirl, M., and Prahl, U. (2024). Twin-roll casting defects in light metals. *J. Mater Sci.* 59, 19003–19022. doi:10.1007/s10853-024-10211-8

Uppal, G., Thakur, A., Chauhan, A., and Bala, S. (2022). Magnesium based implants for functional bone tissue regeneration – a review. *J. Magnesium Alloys* 10, 356–386. doi:10.1016/j.jma.2021.08.017

Wang, X., Du, Y., Liu, D., and Jiang, B. (2020). Significant improvement in mechanical properties of Mg-Zn-La alloy by minor Ca addition. *Mater. Charact.* 160, 110130. doi:10.1016/j.matchar.2020.110130

Yang, L., Liu, G., Ma, L., Zhang, E., Zhou, X., and Thompson, G. (2018). Effect of iron content on the corrosion of pure magnesium: critical factor for iron tolerance limit. *Corros. Sci.* 139, 421–429. doi:10.1016/j.corsci.2018.04.024

Zecevic, M., Beyerlein, I. J., and Knezevic, M. (2018). Activity of pyramidal I and II <c+a> slip in Mg alloys as revealed by texture development. *J. Mech. Phys. Solids* 111, 290–307. doi:10.1016/j.jmps.2017.11.004

Zhang, C., Wu, D., He, Y., Pan, W., Wang, J., and Han, E. (2023). Twinning behavior, microstructure evolution and mechanical property of random-orientated ZK60 Mg alloy compressed at room temperature. *Mater. (Basel)* 16, 1163. doi:10.3390/ma16031163

Zimina, M., Šlapáková, M., Bohlen, J., Letzig, D., Kurz, G., Zaunschirm, S., et al. (2018). Center line segregation in twin-roll cast AZ31 magnesium alloy. *Acta Phys. Pol. A* 134, 774–778. doi:10.12693/APhysPolA.134.774